Feedforward Active Noise Controller Design in Ducts Without Independent Noise Source Measurements

Jwusheng Hu and Jyh-Feng Lin

***Abstract*—Feedforward control architectures have been widely used in active noise control systems to achieve broad-band noise reductions. The basic principle of the control algorithm requires that the feedforward signal, usually the noise source, be independent from the actuator's output. Failure to meet this requirement implies that the overall system contains an acoustic feedback loop and stability and robustness issues become important. This paper investigates this problem in a one-dimensional sound field (e.g., ducts) using a unidirectional sound wave as the feedforward signal. Controller design based on a distributed parameter model is studied. Several experiments are conducted to illustrate the design procedure as well as verify the effectiveness of broad-band noise reductions.**

***Index Terms*—Acoustic noise, distributed parameter systems, feedforward systems, frequency domain analysis, propagation.**

I. Introduction

THE idea of active noise cancellation (ANC) was first raised by Lueg in 1936 [15] and has received much attention since the 1980's due to the availability of fast and cost-effective electronics [16]. To achieve a broad-band performance, feedforward control architectures are usually employed. A typical schematic diagram of feedforward duct noise control is shown in Fig. 1.

If the feedforward signal is independent of the control signal (i.e., f_1), many feedforward types of control algorithms can be applied [e.g., least mean squares (LMS) [22], or model matching [11]]. However, when an independent signal is difficult to obtain (e.g., wind noise), the most commonly used approach is to install feedforward sensors at upstream locations (i.e., f_2). As a result, from a control system viewpoint, the structure is no longer a pure feedforward one because the feedforward signal contains the feedback part from the control signal (called acoustic feedback). Therefore, modifications to the control algorithm must be made in order to maintain stability.

Removing the influence of acoustic feedback is a very practical problem. Earlier work was geared toward generating a unidirectional sound wave either from microphone measurements or a multiple actuator arrangement [4], [2], [13], [19]. Another direction is to apply digital signal processing techniques to either subtract the acoustic feedback signal from the sensor measurement directly (called feedback neutralization [21]) or compensate for its influence (the Filter-U algorithm [3]). The latter one requires knowing the dynamics of the feedback path. An on-line identification is not easy since the measurement contains the noise signal, which highly depends on the input (i.e., the actuator's output) to the path. Second, the parameter space associated with these algorithms is usually quite large which may induce problems such as slow convergence and parameter drift (see [14]).

Manuscript received May 28, 1998; revised June 29, 1999. Recommended by Associate Editor, C. C. Lee. This work was supported by the National Science Council of Taiwan under Grant NSC 86-2212-009-008 and TECO Electric Machinery Co. Ltd.

The authors are with the Department of Electrical and Control Engineering, College of Electrical and Computer Engineering, National Chiao-Tung University, Hsinchu, Taiwan (e-mail: jshu@cn.nctu.edu.tw).

Publisher Item Identifier S 1063-6536(00)03186-9.

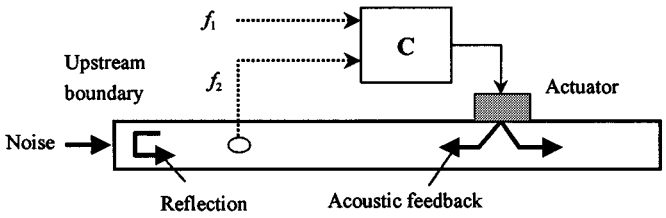

Fig. 1 A schematic diagram of the feedforward noise control in ducts.

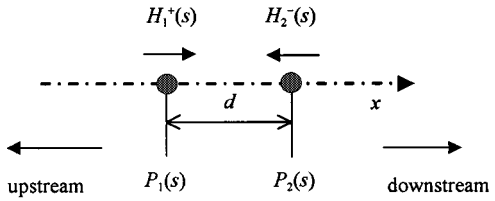

Fig. 2. A two-microphone measurement in a one-dimensional field where $P_1(s)$ and $P_2(s)$ are the Laplace transforms of the measured signals d is the distance between microphones, $H_1^+(s)$ is the wave propagating downstream at microphone 1's location, and $H_2^-(s)$ is the wave propagating upstream at microphone 2's location.

At first glance, obtaining a unidirectional sound measurement does not solve the acoustic feedback problem completely because the wave generated by the actuator also propagates downstream (i.e., reflection from the boundary, see Fig. 1). It can only eliminate the first path. However, it has been shown [10] that under ideal conditions, the reflection has no effect on the cancellation principle. Second, there are limitations to generate unidirectional sound measurements by using ordinary microphones. Consider a two-microphone measurement in a one-dimensional (1-D) field as shown in Fig. 2. From Fig. 2, the microphone measurements are

$$\begin{aligned} P_1(s) &= H_1^+(s) + e^{-\frac{d}{c}s} H_2^-(s) \\ P_2(s) &= e^{-\frac{d}{c}s} H_1^+(s) + H_2^-(s) \end{aligned} \tag{1.1}$$

where c is the speed of sound. Then both upstream and downstream propagating waves can be solved as

$$H_1^+(s) = \frac{P_1(s) - e^{-\frac{d}{c}s}P_2(s)}{1 - e^{-\frac{2d}{c}s}}$$
$$H_2^-(s) = \frac{P_2(s) - e^{-\frac{d}{c}s}P_1(s)}{1 - e^{-\frac{2d}{c}s}}. \quad (1.2)$$

Equation (1.2) shows that at certain frequencies ($\omega = nc\pi/d,\ n = 1,2,\cdots$), the transfer functions are unstable (or marginally stable). In practice, the distance d can be selected to constrain the control bandwidth below $\omega_N = c\pi/d$, much like the scenario in digital control. However, as shown in this paper, this does not guarantee stability unless a modification is done. The analysis can be easily extended to an arbitrary number of sensors. Essentially, singularities occur at integer-multiples of the distances of all sensor pairs. Unless the distances are all irrational numbers, the situation cannot be avoided.

The term "feedforward" in ANC usually means the control signal is synthesized from the noise measurement before its arrival at the actuator's location. However, if independent feedforward signals cannot be obtained, the overall control architecture is actually a very delicate feedback system regardless of the types of algorithms applied. Unfortunately, there is not much work in the control field to analyze these problems. Most research applying standard control design techniques for ANC tend to focus on designing feedback controllers [9], [7], [12], [18], [5]. Roughly speaking, the feedforward algorithms mentioned above have a fundamental difference in the plant's model. The approach of generating unidirectional waves observes the wave propagation properties, which are characterized by distributed dynamics. On the other hand, lumped parameter dynamics are treated when applying digital signal processing techniques. An interesting point about generating unidirectional waves in ducts is that, theoretically, the control law and its performance is independent of the boundary conditions and duct's length. It implies that the control method should have a certain degree of robustness (e.g., under different boundaries).

In this paper, we will discuss the limitations and modifications of using unidirectional wave signals for noise cancellation in ducts in a more rigorous control system design manner. To simplify the problem, a two-sensor configuration (Fig. 2) is assumed. Experimental results are also presented to demonstrate the effect of noise reduction and the robustness of the control system.

II. System Modeling

Consider an active duct noise control system as shown in Fig. 3. Using the one-dimensional approximation, the duct's response can be modeled by solving for the Green's function of the wave equation as (see [8] for more detail)
when $x \geq x_a$ (downstream segment with regard to x_a)

$$\left(1 - \theta_0(s)\theta_1(s)e^{-\frac{2s}{c}L}\right)\bar{Y}(x,s) = (G_D^+(x,x_d,s) + G_D^-(x,x_d,s))\bar{N}(s) + (G_D^+(x,x_a,s) + G_D^-(x,x_a,s))\bar{U}_1(s) \quad (2.1a)$$

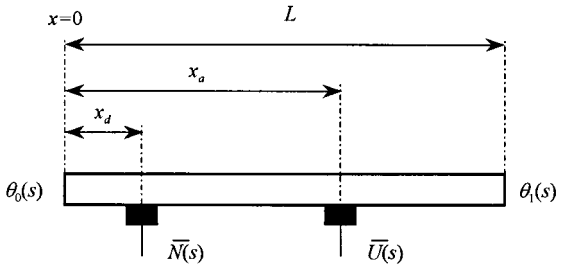

Fig. 3. A finite-length duct with length L, $\bar{N}(s)$ the noise signal (primary source), $\bar{U}(s)$ the control signal (secondary source), and $\theta_0(s)$ and $\theta_1(s)$ the boundary reflection coefficients.

and when $x_a \geq x > x_d$ (upstream segment)

$$\left(1 - \theta_0(s)\theta_1(s)e^{-\frac{2s}{c}L}\right)\bar{Y}(x,s) = (G_D^+(x,x_d,s) + G_D^-(x,x_d,s))\bar{N}(s) + (G_U^+(x,x_a,s) + G_U^-(x,x_a,s))\bar{U}_1(s) \quad (2.1b)$$

where $\bar{U}_1(s) = \bar{Q}_{\mathrm{MS}}(s)\bar{U}(s)$, and $\bar{Q}_{\mathrm{MS}}(s)$ denotes the dynamics of the sensors (e.g., microphones), actuators (e.g., speakers) and electronic components, and

$$G_D^+(x,x',s) = \left[-e^{-\frac{s}{c}(x-x')} + \theta_0(s)e^{-\frac{s}{c}(x+x')}\right] \quad (2.1c)$$

$$G_D^-(x,x',s) = \left[\theta_1(s)e^{-\frac{s}{c}(2L-x-x')} - \theta_0(s)\theta_1(s)e^{-\frac{s}{c}(2L+x'-x)}\right] \quad (2.1d)$$

$$G_U^+(x,x',s) = \left[\theta_0(s)e^{-\frac{s}{c}(x+x')} - \theta_0(s)\theta_1(s)e^{-\frac{s}{c}(2L+x-x')}\right] \quad (2.1e)$$

$$G_U^-(x,x',s) = \left[-e^{-\frac{s}{c}(x-x')} + \theta_1(s)e^{-\frac{s}{c}(2L-x-x')}\right] \quad (2.1f)$$

The notations on the left-hand sides of (2.1c) to (2.1f) are designed to represent the physical meanings of the right-hand sides accordingly. Namely, subscript "D" means a downstream location (the duct's section of $x \geq x'$) while "U" means an upstream one ($x < x'$). Second, the superscript "$+$" means wave propagating in the downstream direction and "$-$" in the upstream direction. The representation can be easily checked by investigating the delay operators. Finally, it can be verified that (2.1c) to (2.1f) satisfy the following relations:

$$G_D^+(x,x_d,s)G_D^+(y,x_a,s) - G_D^+(x,x_a,s)G_D^+(y,x_d,s) = 0 \quad (2.2a)$$

$$G_D^-(x,x_d,s)G_D^+(y,x_a,s) - G_D^-(x,x_a,s)G_D^+(y,x_d,s) = 0 \quad (2.2b)$$

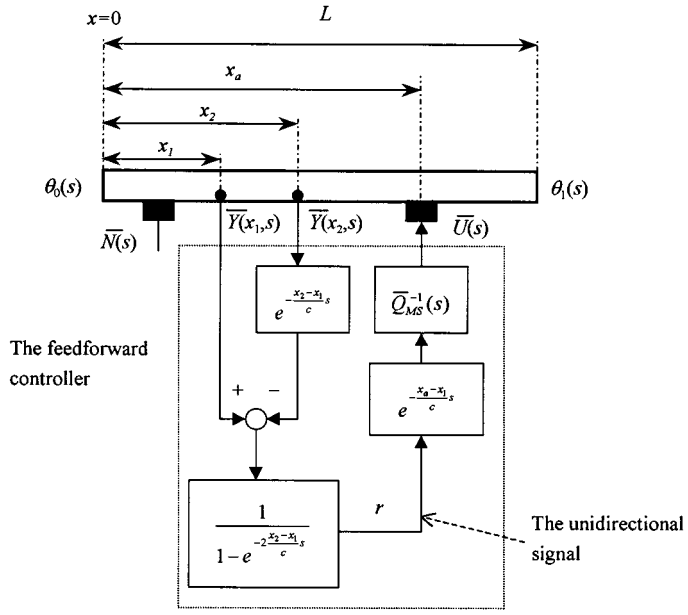

Fig. 4. The feedforward control system using a two-microphone measurement.

III. The Feedforward Control System

An ideal structure of feedforward control, as shown in Fig. 4, consists of a unidirectional signal r, a delay element and an ideal compensation filter $\bar{Q}_{\rm MS}^{-1}(s)$. Fig. 4 is nothing but feeding a delayed downstream propagating wave (recovered at x_1) into the actuator $\bar{U}(s)$ directly. It is easy to see that if the boundary reflection coefficient $\theta_0(s)$ is zero (i.e., a semi-infinite duct), the acoustic feedback signal from the actuator $\bar{U}(s)$ has no effect on r. Therefore, the principle of cancellation is applied. To explain that this configuration still works for a nonzero $\theta_0(s)$ is a little bit subtle. To begin with, assume first that $\bar{Q}_{\rm MS}^{-1}(s)$ exists. The controller of Fig. 4 takes the following form:

$$\bar{U}(s) = \frac{\left[\bar{Y}(x_1,s)-\bar{Y}(x_2,s)e^{-\frac{s}{c}(x_2-x_1)}\right]e^{-\frac{s}{c}(x_a-x_1)}}{1-e^{-\frac{2s}{c}(x_2-x_1)}}\bar{Q}_{\rm MS}^{-1}(s) \tag{3.1}$$

Using (2.1b), the recovered downstream propagating wave can be written as

$$\frac{\left[\bar{Y}(x_1,s)-\bar{Y}(s_2,s)e^{-\frac{s}{c}(x_2-x_1)}\right]}{\left[1-e^{-\frac{2s}{c}(x_2-x_1)}\right]} = \frac{(G_U^+(x_1,x_a,s)\bar{Q}_{\rm MS}(s)\bar{U}(s)G_D^+(x_1,x_d,s)\bar{N}(s))}{\left(1-\theta_0(s)\theta_1(s)e^{-\frac{2s}{c}L}\right)} \tag{3.2}$$

Combining (3.1) and (3.2), the control signal satisfies the following equation:

$$\bar{Q}_{\rm MS}(s)\bar{U}(s) = e^{-\frac{s}{c}(x_a-x_1)} \times \frac{\left(G_U^+(x_1,x_a,s)\bar{Q}_{\rm MS}(s)\bar{U}(s)+G_D^+(x_1,x_d,s)\bar{N}(s)\right)}{\left(1-\theta_0(s)\theta_1(s)e^{-\frac{2s}{c}L}\right)} \tag{3.3}$$

Further, it can be verified from (2.1e) that

$$\begin{aligned} 1-\theta_0(s)\theta_1(s)e^{-\frac{2s}{c}L}-e^{-\frac{s}{c}(x_a-x_1)}G_U^+(x_1,x_a,s) &= 1-\theta_0(s)e^{-\frac{2s}{c}x_a} \\ &= -e^{\frac{s}{c}(y-x_a)}\left(-e^{-\frac{s}{c}(y-x_a)}+\theta_0(s)e^{-\frac{s}{c}(y+x_a)}\right) \\ &= -e^{\frac{s}{c}(y-x_a)}G_D^+(y,x_a,s), \quad \forall y>x_a \end{aligned} \tag{3.4}$$

Combining (3.3) and (3.4) and using the fact that

$$G_D^+(y,x_d,s) = e^{-(y-x_1)s/c}G_D^+(x_1,x_d,s), \quad \forall y>x_1$$

we have an alternative representation of the controller as

$$\bar{Q}_{\rm MS}(s)\bar{U}(s) = \frac{-G_D^+(y,x_d,s)}{G_D^+(y,x_a,s)}\bar{N}(s), \quad \forall y, \quad y>x_a \tag{3.5}$$

Equation (3.5) shows that the control law of (3.1) equivalently cancels the downstream propagating wave of the noise. Applying (3.5) to (2.1a) and using the properties of (2.2a) and (2.2b), the downstream response becomes

$$\left(1-\theta_0(s)\theta_1(s)e^{-\frac{2s}{c}L}\right)\bar{Y}(y,s)=0, \quad \forall y>x_a. \tag{3.6}$$

Second, the upstream response after applying the controller is as shown in (3.7) at the bottom of the page (please see [10]), $\forall x_d<y<x_a$. It can be verified that (3.7), shown at the bottom of the page, is exactly the solution of a duct whose length is x_a and boundary reflection coefficients are $\theta_0(s)$ at $y=0$ and 1 at $y=x_a$. In other words, a total reflection is achieved at the actuator's location.

Equations (3.6) and (3.7) give the ideal closed-loop response from disturbance to output. Therefore, to guarantee both performance and stability, the characteristic roots of both $1-\theta_0(s)\theta_1(s)e^{-(2s/c)L}=0$ and $1-\theta_0(s)e^{-(2s/c)x_a}=0$ must lie on the left-hand side of the complex plane. These in turn are satisfied if the following assumptions were observed.

Assumption 3.1: $\theta_0(s)$ and $\theta_1(s)$ are stable, proper rational transfer functions, and

$$|\theta_0(j\omega)|<1 \quad \text{and} \quad |\theta_1(j\omega)|<1, \quad \forall \omega>0.$$

This assumption applies to passive boundaries where the impedance functions are strictly positive real (see [17]).

$$\bar{Y}(y,s) = \frac{-e^{-\frac{s}{c}(y-x_d)}+\theta_0(s)e^{-\frac{s}{c}(y+x_d)}+e^{-\frac{s}{c}(2x_a-x_d-y)}-\theta_0(s)e^{-\frac{s}{c}(2x_a+x_d-y)}}{1-\theta_0(s)e^{-\frac{2s}{c}x_a}}\bar{N}(s). \tag{3.7}$$

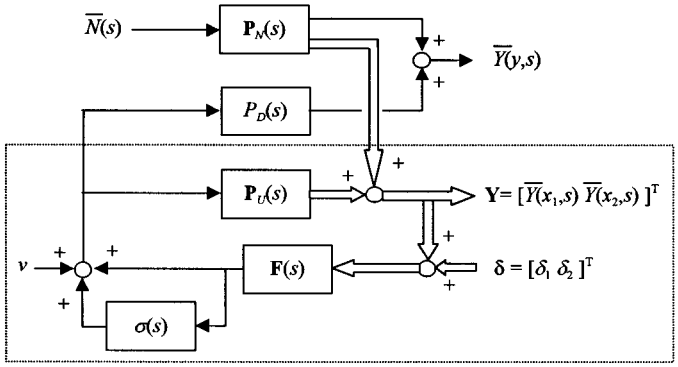

Fig. 5. Block diagram of the feedforward control system.

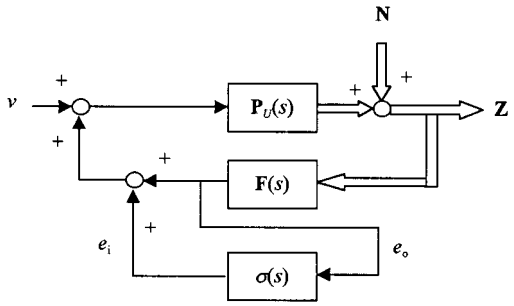

Fig. 6 The block diagram for the stability analysis of Fig. 5.

IV. Stability Analysis and Controller Modification

Although the effectiveness of the simple control law can be justified theoretically, it faces several challenges when implemented. The main issue is the stability problem induced from measurement noise and model uncertainty. From (3.1), the parameters required to calculate the control law are two delay periods and the compensation filter. In this paper, we only consider the uncertainty of the filter because it is unlikely to implement a precise inverse of $\bar{Q}_{\rm MS}(s)$ (e.g., identification errors or nonminimum phase zeros). Let δ_1 and δ_2 be the measurement errors of $\bar{Y}(x_1,s)$ and $\bar{Y}(x_2,s)$, respectively, ν the input noise (e.g., quantization error), and $C(s)$ a stable approximation of $\bar{Q}_{\rm MS}^{-1}(s)$ with a stable additive uncertainty $\sigma(s)$ as

$$C(s)\bar{Q}_{\rm MS}(s)=1+\sigma(s). \tag{4.1}$$

The closed-loop control system described in the preceding section can be arranged in the block diagram shown in Fig. 5. From (2.1a) and (2.1b), each composition of the block diagram can be found to be

$$\mathbf{P}_N(s)=\frac{1}{\Delta(s)}\begin{bmatrix} G_D^+(y,x_d,s)+G_D^-(y,x_d,s)\\ G_D^+(x_1,x_d,s)+G_D^-(x_1,x_d,s)\\ G_D^+(x_2,x_d,s)+G_D^-(x_2,x_d,s)\end{bmatrix} \tag{4.2}$$

$$P_D(s)=\frac{1}{\Delta(s)}(G_D^+(y,x_a,s)+G_D^-(y,x_a,s)) \tag{4.3}$$

$$\mathbf{P}_U(s)=\frac{1}{\Delta(s)}\begin{bmatrix} G_U^+(x_1,x_a,s)+G_U^-(x_1,x_a,s)\\ G_U^+(x_2,x_a,s)+G_U^-(x_2,x_a,s)\end{bmatrix} \tag{4.4}$$

$$\mathbf{F}(s)=\frac{e^{-\frac{s}{c}(x_a-x_1)}}{1-e^{-\frac{2s}{c}(x_2-x_1)}}\begin{bmatrix}1\\ -e^{-\frac{s}{c}(x_2-x_1)}\end{bmatrix}^T \tag{4.5}$$

and

$$\Delta(s)=1-\theta_0(s)\theta_1(s)e^{-\frac{2s}{c}L}. \tag{4.6}$$

For stability we need to consider the dynamics enclosed by the dotted line in Fig. 5 (see Fig. 6). The input–output map of Fig. 6 can be derived as

$$\begin{bmatrix}\mathbf{Z}\\ e_o\end{bmatrix}=(1-\mathbf{F}(s)\mathbf{P}_U(s))^{-1}\times\begin{bmatrix}\mathbf{I}_2 & \mathbf{P}_U(s) & \mathbf{P}_U(s)\\ \mathbf{F}(s) & \mathbf{F}(s)\mathbf{P}_U(s) & \mathbf{F}(s)\mathbf{P}_U(s)\end{bmatrix}\begin{bmatrix}\mathbf{N}\\ \nu\\ e_i\end{bmatrix}. \tag{4.7}$$

In the absence of model uncertainty (i.e., $\sigma(s)=0$ in Fig. 6), the closed-loop system is bounded input–bounded output (BIBO) stable if and only if $(1-\mathbf{F}(s)\mathbf{P}_U(s))^{-1}\mathbf{F}(s)$ is BIBO stable (since $\mathbf{P}_U(s)$ is stable by Assumption 3.1). Now

$$\begin{aligned}&(1-\mathbf{F}(s)\mathbf{P}_U(s))^{-1}\mathbf{F}(s)\\ &\quad=\frac{1-\theta_0(s)\theta_1(s)e^{-\frac{2s}{c}L}}{1-\theta_0(s)e^{-\frac{2s}{c}x_a}}\cdot\frac{e^{-\frac{s}{c}(x_a-x_1)}}{1-e^{-\frac{2s}{c}(x_2-x_1)}}\\ &\qquad\times\begin{bmatrix}1\\ -e^{-\frac{s}{c}(x_2-x_1)}\end{bmatrix}^T.\end{aligned} \tag{4.8}$$

Due to poles located on the imaginary axis, the closed-loop feedback block diagram in Fig. 6 is not stable. As stated in Section I, these poles are singular points when constructing unidirectional waves. Obviously the performance at those frequencies have to be sacrificed. From (4.8), the controller $\mathbf{F}(s)$ is modified by adding a "notch filter," $R_\varepsilon(s)$, i.e.,

$$\mathbf{F}_m(s)=\mathbf{F}(s)R_\varepsilon(s) \tag{4.9}$$

where

$$R_\varepsilon(s)=\frac{1-e^{-\frac{2s}{c}(x_2-x_1)}}{1-(1-k\varepsilon(s))e^{-\frac{2s}{c}(x_2-x_1)}},\quad \text{Real}\,\{\varepsilon(j\omega)\}>0,\ k>0\ \text{ and }\ \|k\varepsilon(s)\|\ll 1. \tag{4.10}$$

It is obvious that $\mathbf{F}_m(s)$ is stable if the following condition is satisfied:

$$0<k<\inf_{\omega>0}\left[\frac{1}{\varepsilon(j\omega)}+\frac{1}{\varepsilon(-j\omega)}\right] \tag{4.11}$$

By making $F_m(s)$ a stable filter, the closed-loop system of Fig. 6 is stable if and only if $(1-\mathbf{F}_m(s)\mathbf{P}_U(s))^{-1}$ is stable, i.e.,

$$\begin{aligned}(1-\mathbf{F}_m(s)\mathbf{P}_U(s))^{-1} &= \left(1-(1-k\varepsilon(s))e^{-\frac{2s}{c}(x_2-x_1)}\right)T(s) \\ &\cdot \frac{1}{\left[1-(1-k\varepsilon(s)T(s))e^{-\frac{2s}{c}(x_2-x_1)}\right]} \end{aligned} \quad (4.12)$$

where

$$T(s)=\frac{1-\theta_0(s)\theta_1(s)e^{-\frac{2s}{c}L}}{1-\theta_0(s)e^{-\frac{2s}{c}x_a}}. \quad (4.13)$$

For analysis, (4.12) can be arranged as Fig 7. Since $T(s)$ is stable by Assumption 3.1, using the small-gain theorem the closed-loop system of Fig. 7 is BIBO stable if $\|1-k\varepsilon(s)T(s)\|<1$ where $\|\cdot\|$ denotes the infinity norm. This requires that $\varepsilon(j\omega)T(j\omega)$ lies in the right-hand side of the complex plane. In other words, $\varepsilon(s)$ is responsible for compensating the phase of $T(s)$. Denoting $T_\varepsilon(s)=\varepsilon(s)T(s)$, the upper bound of k, denoted by $\bar{k}$, can be easily found as

$$0<k<\bar{k},\quad \bar{k}=\min\left\{\inf_{\omega>0}\left[\frac{1}{\varepsilon(j\omega)}+\frac{1}{\varepsilon(-j\omega)}\right]\right. \\ \left.\inf_{\omega>0}\left[\frac{1}{T_\varepsilon(j\omega)}+\frac{1}{T_\varepsilon(-j\omega)}\right]\right\}. \quad (4.14)$$

We summarize the stability analysis in the following lemma.

Lemma 4.1: Under Assumption 3.1, the closed-loop system of Fig. 7 is BIBO stable if $\mathrm{Real}\{\varepsilon(j\omega)\}>0$, $\mathrm{Real}\{\varepsilon(j\omega)T(j\omega)\}>0$ and (4.14) hold.

Remark 4.1: A model-based design of the compensation filter $\varepsilon(s)$ may not be easy since $T(s)$ is distributed in nature. Alternatively, if the phase of $T(j\omega)$ is confined in a small region, we can design $\varepsilon(s)$ by using a simple phase lead/lag filter. Notice that if the following condition holds [see (4.13)], we have $\mathrm{Real}\{T(j\omega)\}>0$:

$$\sup_{\omega>0}\left(\angle\left(1-\theta_0(j\omega)\theta_1(j\omega)e^{-\frac{2\omega j}{c}L}\right)\right. \\ \left.-\angle\left(1-\theta_0(j\omega)e^{-\frac{2\omega j}{c}x_a}\right)\right)<\frac{\pi}{2}. \quad (4.15)$$

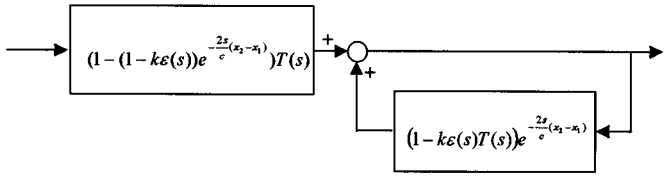

Fig. 7 A closed-loop block diagram equivalent to $(1-\mathbf{F}_m(s)\mathbf{P}_U(s))^{-1}$.

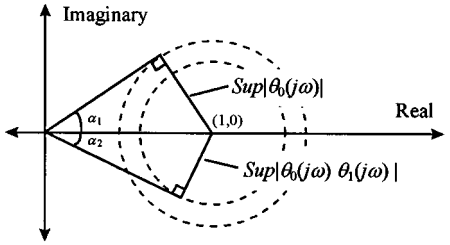

Fig. 8. The possible maximum difference between $\angle(1-\theta_0(j\omega)e^{-(2\omega j/c)x_a})$ and $\angle(1-\theta_0(j\omega)\theta_1(j\omega)e^{-(2\omega j/c)L})$.

A sufficient condition to satisfy the equation above is shown graphically in Fig. 8 and this results in the following constraint on boundary reflection coefficients:

$$\sin^{-1}\|\theta_0(j\omega)\|+\sin^{-1}(\|\theta_0(j\omega)\theta_1(j\omega)\|)=\alpha_1+\alpha_2<\frac{\pi}{2}. \quad (4.16)$$

Equation (4.16) is always true if $\|\theta_0(j\omega)\|<1/\sqrt{2}$ since $\|\theta_0(j\omega)\|<1$ by Assumption 3.1. In other words, making $\theta_0(j\omega)$ small (i.e., more absorption of reflected wave) limits the phase of $T(j\omega)$ and consequently reduces the effort of designing $\varepsilon(s)$. Second, a better robustness property can be obtained when the application requires downstream boundary changes (e.g., outlet airflow control of an air conditioning duct).

Remark 4.2: To determine $T(s)$ experimentally, observe first that the transfer function at a downstream location x is shown in (4.17) at the bottom of the page [see (2.1a)] Taking measurements at two distinct locations x_1 and x_2, we have

$$\begin{bmatrix} e^{-\frac{s}{c}x_1} & e^{\frac{s}{c}x_1} \\ e^{-\frac{s}{c}x_2} & e^{\frac{s}{c}x_2}\end{bmatrix}\begin{bmatrix}1/T(s)\\ \eta(s)\end{bmatrix}=\begin{bmatrix}-e^{-\frac{s}{c}x_a}\frac{H(x_1,s)}{\bar{Q}_{\mathrm{MS}}(s)}\\ -e^{-\frac{s}{c}x_a}\frac{H(x_2,s)}{\bar{Q}_{\mathrm{MS}}(s)}\end{bmatrix}. \quad (4.18)$$

As long as the matrix on the left-hand side of (4.18) is well-conditioned (e.g., frequency range between zero and $\pi c/|x_1-x_2|$), $1/T(j\omega)$ can be estimated. If more measurements were

$$\begin{aligned}H(x,s)=\frac{\bar{Y}(x,s)}{\bar{U}(s)} &= \frac{-e^{-\frac{s}{c}(x-x_a)}\left(1-\theta_0(s)e^{-\frac{2s}{c}x_a}\right)\left(1-\theta_1(s)e^{-\frac{2s}{c}(L-x)}\right)}{\left(1-\theta_0(s)\theta_1(s)e^{-\frac{2s}{c}L}\right)}\bar{Q}_{\mathrm{MS}}(s) \\ &= -e^{\frac{s}{c}x_a}\left(e^{-\frac{s}{c}x}-\theta_1(s)e^{-\frac{2s}{c}L}e^{\frac{s}{c}x}\right)\frac{1}{T(s)}\bar{Q}_{\mathrm{MS}}(s) \end{aligned} \quad (4.17)$$

taken, optimal estimation such as the least-squares method can be applied.

Remark 4.3: The performance degradation depends on the size of $||k\varepsilon(s)||$ [(4.10)]. Specifically, the residual downstream noise can be calculated by replacing $\mathbf{F}(s)$ with $F_m(s)$ in Fig. 5 as

$$\bar{Y}(x,s) = \bar{Y}_d(x,s) \times \xi_1(s) + \xi_2(s), \quad x > x_a$$

where

$$\bar{Y}_d(x,s) = \frac{(G_D^+(x,x_d,s) + G_D^-(x,x_d,s))}{1 - \theta_0(s)\theta_1(s)e^{-\frac{2s}{c}L_x}}$$

$$\xi_1(s) = \frac{k\varepsilon(s)T(s)e^{-\frac{2s}{c}(x_2-x_1)}}{1 - [1 - k\varepsilon(s)T(s)]e^{-\frac{2s}{c}(x_2-x_1)}}$$

and $\xi_2(s)$ is a stable signal proportional to the measurement noise. The signal $\bar{Y}_d(x,s)$ represents the noise before cancellation. Clearly, the degradation ratio $\xi_1(s)$ also depends on $T(s)$ [(4.13)].

For a nonzero model uncertainty $\sigma(s)$ [Fig. 6], it can be shown that the stability of the modified control law depends on (4.19), shown at the bottom of the page. This equation can be further arranged as Fig. 9 similar to Fig. 7. Similarly, using the small-gain theorem the BIBO stability of Fig. 9 can be ensured if $\text{Real}\{T_\varepsilon(j\omega)\} > 0$ where $T_\varepsilon(s) = \varepsilon(s)T(s)$ and

$$||1 - kT_\varepsilon(s)|| < 1 - 2||\sigma(s)||||T(s) - 1||. \tag{4.20}$$

The value of $|1 - kT_\varepsilon(j\omega)|$ in terms of k is plotted in Fig. 10. Clearly, to establish the inequality of (4.20), we must have

$$1 - 2||\sigma(s)||||T(s) - 1|| > \frac{|I_{T_\varepsilon}(\omega)|}{|T_\varepsilon(j\omega)|}$$
$$\text{for every } \omega \text{ where } T_\varepsilon(j\omega) = R_{T\varepsilon}(\omega) + jI_{T\varepsilon}(\omega).$$

Or

$$||\sigma(s)|| < \frac{1}{2||T(s) - 1||}\left(1 - \sup_\omega \frac{|I_{T\varepsilon}(\omega)|}{|T_\varepsilon(j\omega)|}\right). \tag{4.21}$$

Denoting $\bar{\sigma}$ the estimated uncertainty bound and $\gamma_k = 1 - 2\bar{\sigma}||T(s) - 1||$, the bounds on k can be derived as

$$\underline{k} < k < \bar{k} \tag{4.22}$$

where

$$\underline{k} = \sup_\omega \left\{ \frac{1}{|T_\varepsilon(j\omega)|^2}\left(R_{T\varepsilon}(\omega) - \sqrt{|T_\varepsilon(j\omega)|^2\gamma_k^2 - I_{T\varepsilon}(\omega)^2}\right)\right\} \quad \text{and}$$

$$\bar{k} = \text{Min}\left\{ \inf_\omega \left[\frac{1}{\varepsilon(j\omega)} + \frac{1}{\varepsilon(-j\omega)}\right], \inf_\omega \left[\frac{1}{|T_\varepsilon(j\omega)|^2}\left(R_{T\varepsilon}(\omega) + \sqrt{|T_\varepsilon(j\omega)|^2\gamma_k^2 - I_{T\varepsilon}(\omega)^2}\right)\right]\right\}.$$

Lemma 4.2 summarizes the stability conditions in the presence of model uncertainty.

Lemma 4.2: Under Assumption 3.1, the closed-loop system of Fig. 9 is BIBO stable $\text{Real}\{\varepsilon(j\omega)\} > 0$, $\text{Real}\{\varepsilon(j\omega)T(j\omega)\} > 0$ and (4.21) and (4.22) hold.

V. Experimental Verification

An experiment was conducted to verify the feedforward control law. The experimental procedure is summarized in the following steps:

- Step 1) Determine the combined dynamics of speaker and microphone $\bar{Q}_{\text{MS}}(z^{-1})$.
- Step 2) Determine the transfer function $T(s)$ using (4.18). If $\text{Real}\{T(j\omega)\} < 0$, design a filter $\varepsilon(s)$ such that $\text{Real}\{\varepsilon(j\omega)T(j\omega)\} > 0$.
- Step 3) Use $\varepsilon(s), T(s)$ and (4.21) to find the uncertainty bound $|\sigma(s)|$.
- Step 4) Solve the inverse filter $C(z^{-1})$ by the model matching techniques (as explained latter).
- Step 5) Determine the estimated uncertainty bound J (i.e., $\bar{\sigma}$) using (5.6). This bound can be lowered by increasing the distance of $x_a - x_1$.
- Step 6) Use $\bar{\sigma}$ and (4.22) to find the upper and lower bound of k and determine an appropriate value (i.e., midpoint).
- Step 7) Use (5.4) to implement the control law.

A. Identification and Design

Fig. 11 shows the experimental setup. The duct's dimensions are 18 cm × 18 cm × 200 cm and its cutoff frequency for $(0,1)$ or $(1,0)$ mode is about 945 Hz. For frequency smaller than 945 Hz, only the plane-wave mode is propagating. A digital signal processor (DSP)-based system was used to perform real-time

$$[1 - \mathbf{F}_m(s)\mathbf{P}_U(s)(1 + \sigma(s))]^{-1} = \left[1 - (1 - k\varepsilon(s))e^{-\frac{2s}{c}(x_2-x_1)}\right]T(s) \cdot \frac{1}{\left[1 - (1 - k\varepsilon(s)T(s))e^{-\frac{2s}{c}(x_2-x_1)} - \sigma(s)\left(1 - e^{-\frac{2s}{c}(x_2-x_1)}\right)(T(s) - 1)\right]}. \tag{4.19}$$

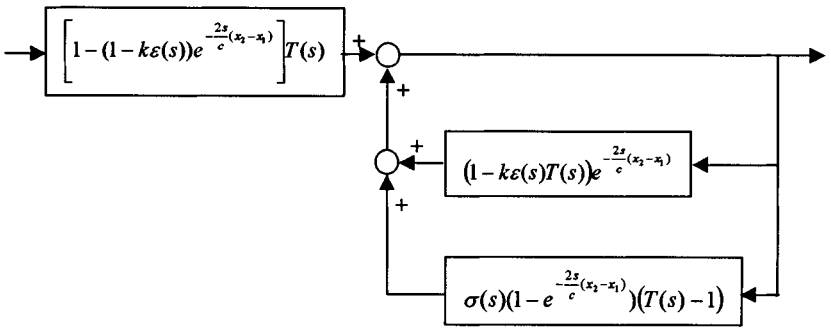

Fig. 9. A closed-loop block diagram equivalent to $[1-\mathbf{F}_m(s)\mathbf{P}_U(s)(1+\sigma(s))]^{-1}$.

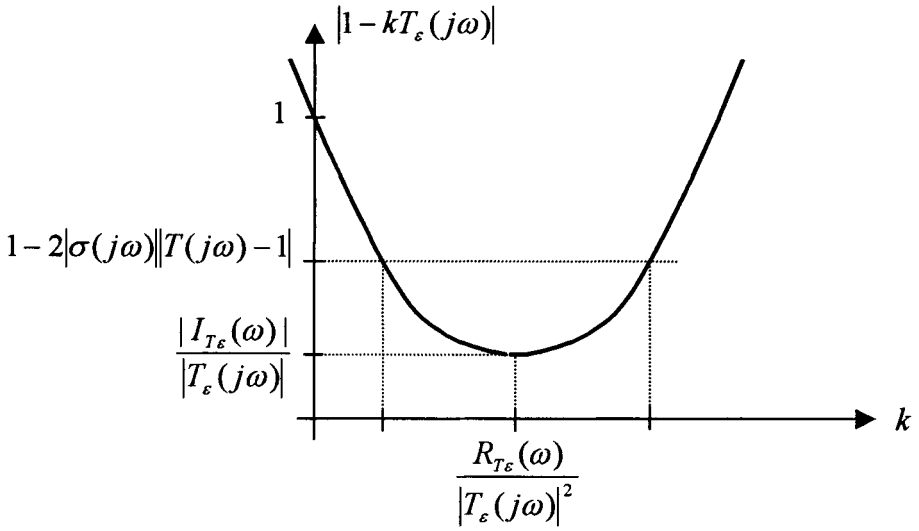

Fig. 10. The plot of $|1-kT_\varepsilon(j\omega)|$ vs, k for every ω where $R_{T\varepsilon}(\omega)$ and $I_{T\varepsilon}(\omega)$ denote the real and imaginary part of $T(j\omega)$.

calculations and the sampling rate was chosen to be 5000 Hz. The loudspeaker's diameter used in this experiment was 16 cm. The design was implemented directly in the digital domain by matching various frequency domain criteria described in previous sections.

The cutoff frequency represents the control bandwidth of the system approximated by a one-dimensional (1-D) wave equation. Although it can be calculated (945 Hz), we are interested to see if it can be found experimentally. To begin with, notice that pure delay operations characterize the wave propagation behavior in the 1-D model. Therefore, if three measurements were taken at y_1, y_2, and y_3 where $y_2-y_1=y_3-y_2>0$, we have

$$e^{-s\tau}(\bar{Y}(y_1,s)+\bar{Y}(y_3,s))=(1+e^{-2s\tau})\bar{Y}(y_2,s)$$

or

$$\frac{\bar{Y}(y_1,s)+\bar{Y}(y_3,s)}{\bar{Y}(y_2,s)}=\frac{1+e^{-2s\tau}}{e^{-s\tau}}=e^{s\tau}+e^{-s\tau}=2\cos(\omega\tau) \tag{5.1}$$

where $\tau=(y_2-y_1)/c$. The left-hand side of (5.1) can be determined experimentally. Fig. 12 shows the verification of this equation by setting $y_1=181.4$ cm, $y_2=188.3$ cm and $y_3=195.2$ cm. Clearly, the 1-D model approximation is no longer accurate beyond 800 Hz. The mismatch between this value and the theoretical one (945 Hz) is probably due to the short distance between the sound source and measurement points where some evanescent modes still have strong influences. Notice that y_1 is selected such that $y_1-x_a<x_a-x_2$ (see Fig. 11). Therefore, by limiting our control bandwidth to 800 Hz, the plane wave model should be an accurate representation to investigate the feedforward control law.

The next step is to determine the combined dynamics of speaker and microphone ($\bar{Q}_{\mathrm{MS}}(s)$ of (2.1). Placing the speaker and microphones in a reflection-free environment (i.e., a full anechoic chamber), $\bar{Q}_{\mathrm{MS}}(s)$ is approximated digitally (at 5 kHz) by a standard least-squares procedure as (see Fig. 13),

$$\begin{aligned}\bar{Q}_{\mathrm{MS}}(z^{-1})=&\frac{(1-1.4820z^{-1}+0.9635z^{-2})}{(1-1.4598z^{-1}+0.9371z^{-2})}\\&\times\frac{(1-1.7141z^{-1}+0.9659z^{-2})}{(1-1.1999z^{-1}+0.6563z^{-2})}\\&\times\frac{(1-1.8546z^{-1}+0.9446z^{-2})}{(1-1.7097z^{-1}+0.9596z^{-2})}\\&\times\frac{(1-4.3320z^{-1}+2.5328z^{-2})}{(1-1.8777z^{-1}+0.9384z^{-2})}\\&\times\frac{-0.012\,87z^{-8}}{(1-1.8275z^{-1}+0.9325z^{-2})}.\end{aligned} \tag{5.2}$$

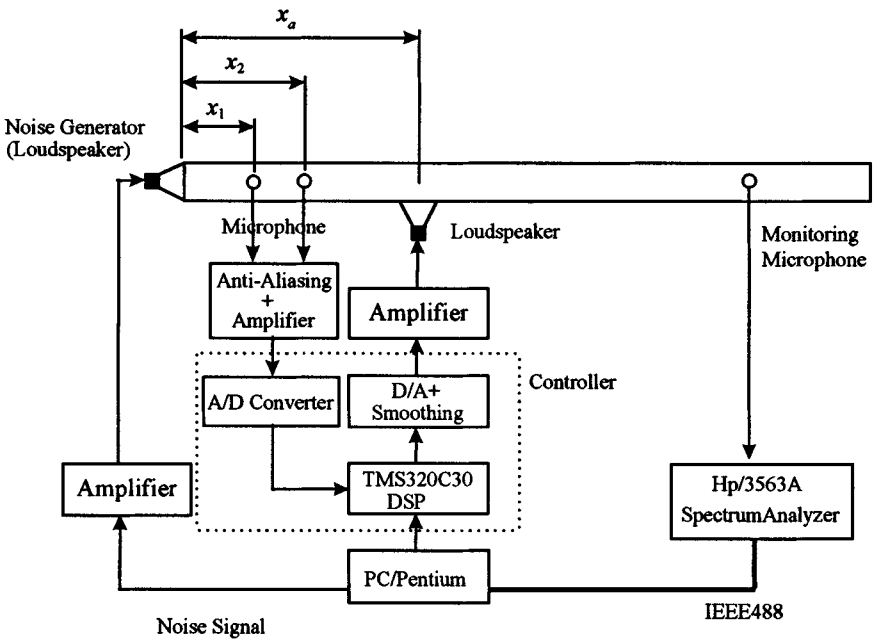

Fig. 11 Block diagram of the control system ($x_1 = 50.3$ cm, $x_2 = 57.2$ cm and $x_a = 140$ cm).

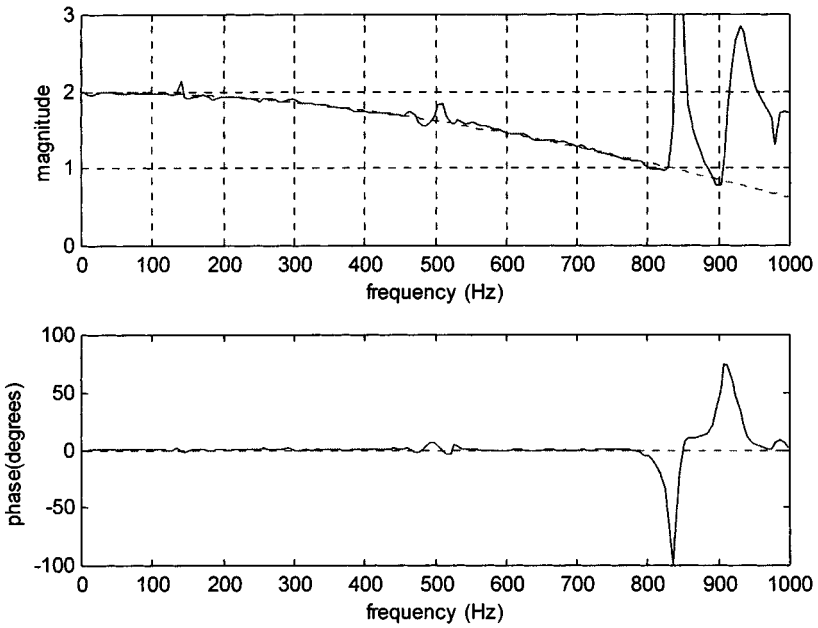

Fig. 12. Experimental verification of the delay operation in the duct described by (5.1) (solid line: experimental data; dashed line theoretical value).

To determine the transfer function $T(s)$ [(4.13)], we used the measurements at y_1, y_2, and y_3 again. By solving (4.18) at each frequency, the frequency response of $T(s)$ is calculated as shown in Fig. 14. The three results match very well between 50 and 800 Hz. Below 50 Hz, the results are not consistent due to the performance limitation of the loudspeaker used in this experiment. However, Fig. 14 shows that, within the bandwidth, the phase of $T(s)$ is confined within $\pm 90°$except in two small regions. The phase compensation filter $\varepsilon(s)$ can be easily found to make $\text{Real}\{\varepsilon(j\omega)T(j\omega)\} > 0$ (see Lemma 4.1 and Remark 4.1). From Fig. 14, $\varepsilon(s)$ should provide phase lag at low frequency region. Fig. 15 shows the phase response of the filters $\varepsilon(s)$ and $\varepsilon(s)T(s)$. A digital filter to match this response is selected as

$$\varepsilon(z^{-1}) = \frac{1 - 0.95z^{-1}}{1 - 0.85z^{-1}}. \tag{5.3}$$

Rewrite again the control law

$$\bar{U}(s) = \frac{\left[\bar{Y}(x_1, s) - \bar{Y}(x_2, s)e^{-\frac{s}{c}(x_2 - x_1)}\right] e^{-\frac{s}{c}(x_a - x_1)}}{1 - [1 - k\varepsilon(s)]e^{-\frac{2s}{c}(x_2 - x_1)}} C(s).$$

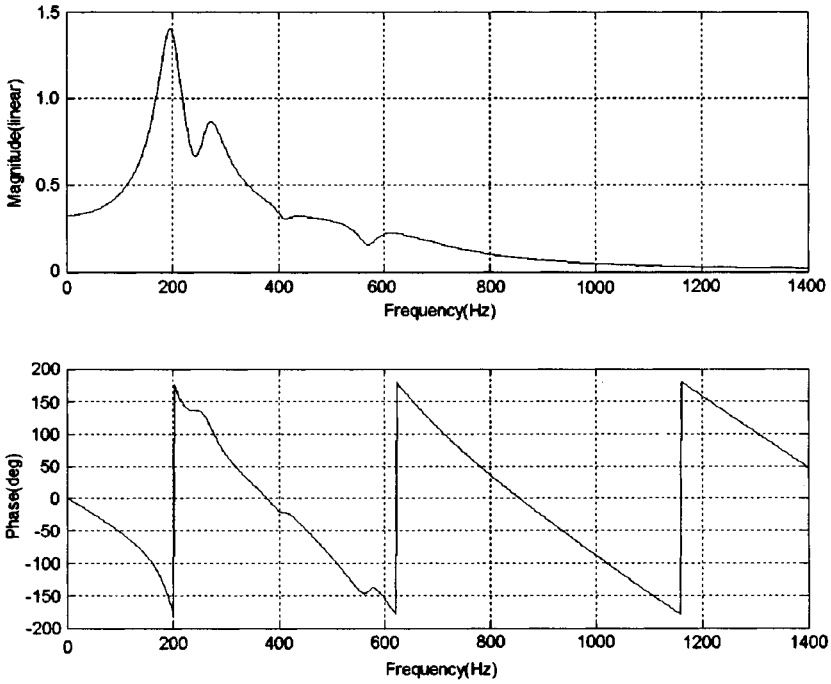

Fig. 13. Magnitude and phase response of $\bar{Q}_{\mathrm{MS}}(z^{-1})$.

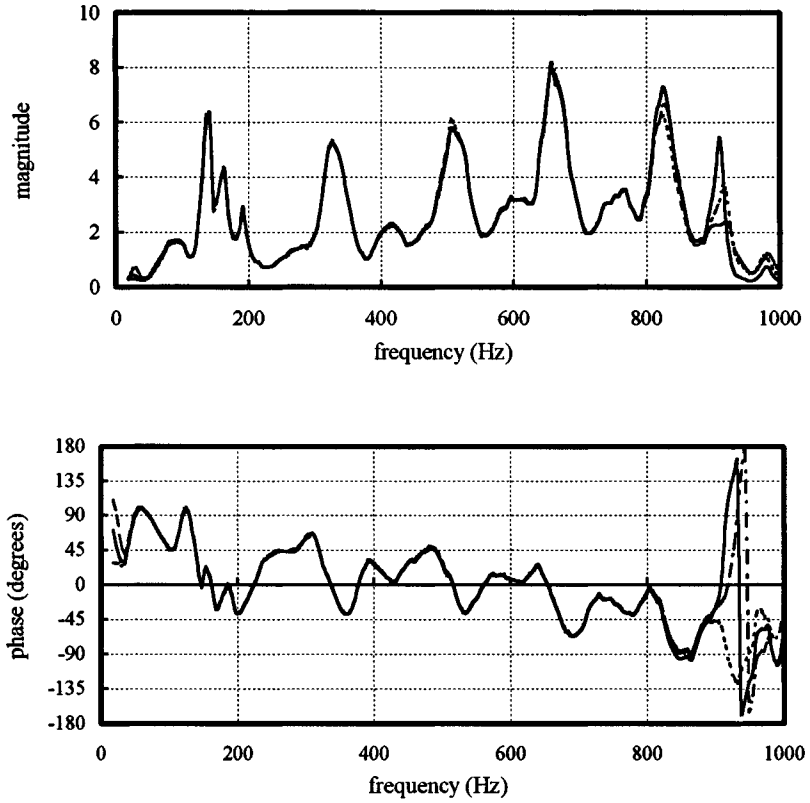

Fig. 14. Bode plot of $T(s)$ calculated by (4.13) and data measured at $y_1 = 181.4$ cm $y_2 = 188.3$ cm and $y_3 = 195.2$ cm (solid line: y_1 and y_2; dashed line: y_2 and y_3; dash-dot line: y_1 and y_3).

Under 5 kHz sampling, $(x_a - x_1)/c$ equals 13 digital delay steps and $(x_2 - x_1)/c$ equals one delay step where $c \approx 345$ m/s. Therefore, the control law is implemented digitally as

$$\bar{U}(z^{-1}) = \frac{[\bar{Y}(x_1, z^{-1}) - z^{-1}\bar{Y}(x_2, z^{-1})]z^{-13}}{1 - [1 - k\varepsilon(z^{-1})]z^{-2}} \tag{5.4}$$

where $C(z^{-1})$ is a stable inverse of $\bar{Q}_{\mathrm{MS}}(z^{-1})$ [(5.2)]. Before calculating $C(z^{-1})$, the uncertainty bound of (4.21) is found first to access the inversion accuracy within the control bandwidth. Using the frequency responses of $\varepsilon(s)$ and $\varepsilon(s)T(s)$, the bound is calculated as

$$\|\sigma(s)\| < 0.0055. \tag{5.5}$$

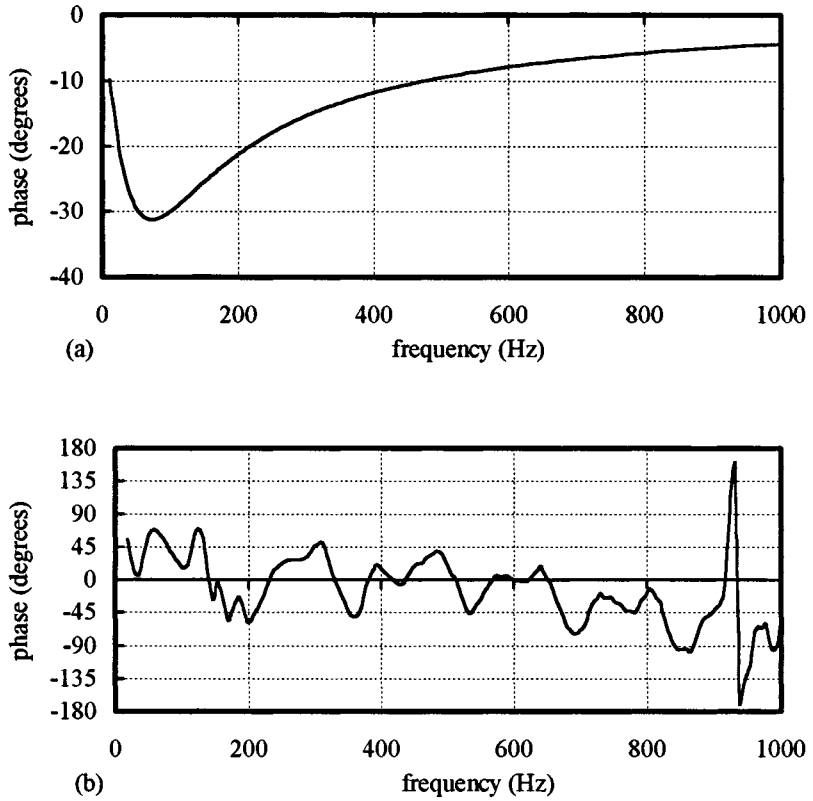

Fig. 15. The phase response of (a) the compensation filter $\varepsilon(s)$; (b) the filter $\varepsilon(s)T(s)$ where $T(s)$ is the average of the data shown in Fig. 14.

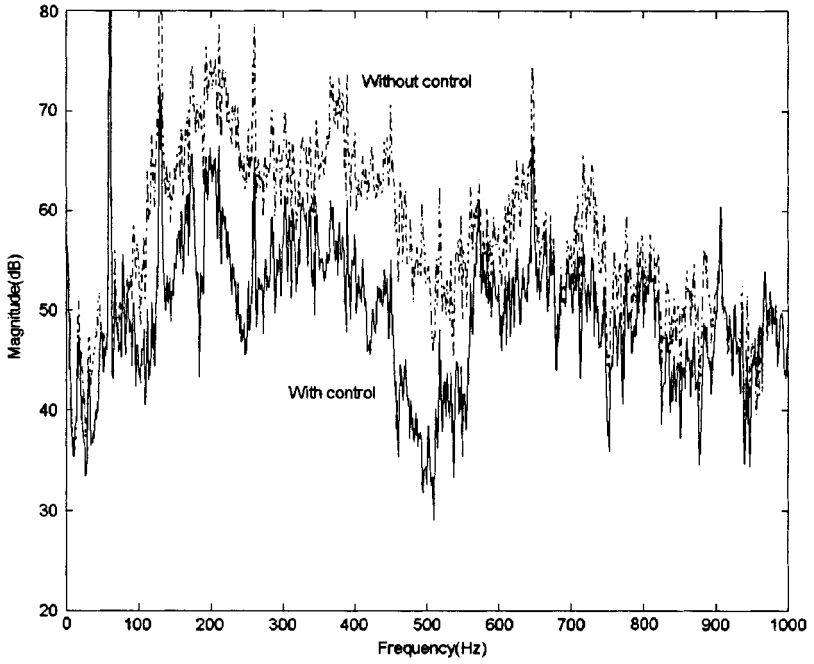

Fig. 16. Broad-band results of the feedforward active control in the duct (open-ended at the downstream boundary).

$C(z^{-1})$ is then solved by the model matching techniques [1], [6]. Notice that (5.4) contains 13 steps of delay, allowing $C(z^{-1})$ to be noncausal with a maximum 13 steps of preview [20] [11]. Therefore, the matching formulation is devised as

$$J = \mathrm{Min}_{C' \in \mathrm{RH}_\infty} \| z^{-13} - \bar{Q}_{\mathrm{MS}}(z^{-1}) C'(z^{-1}) \| \qquad (5.6)$$

where $\| \cdot \|$ denotes the infinity norm and $C'(z^{-1}) = z^{-13} C(z^{-1})$. The optimal solution of $C(z^{-1})$ is then calculated as

$$C(z^{-1}) = 0.1224 z^{13} \frac{(1 - 2.2467 z^{-1} + 13.2152 z^{-2})}{(1 - 1.4820 z^{-1} + 0.9635 z^{-2})}$$

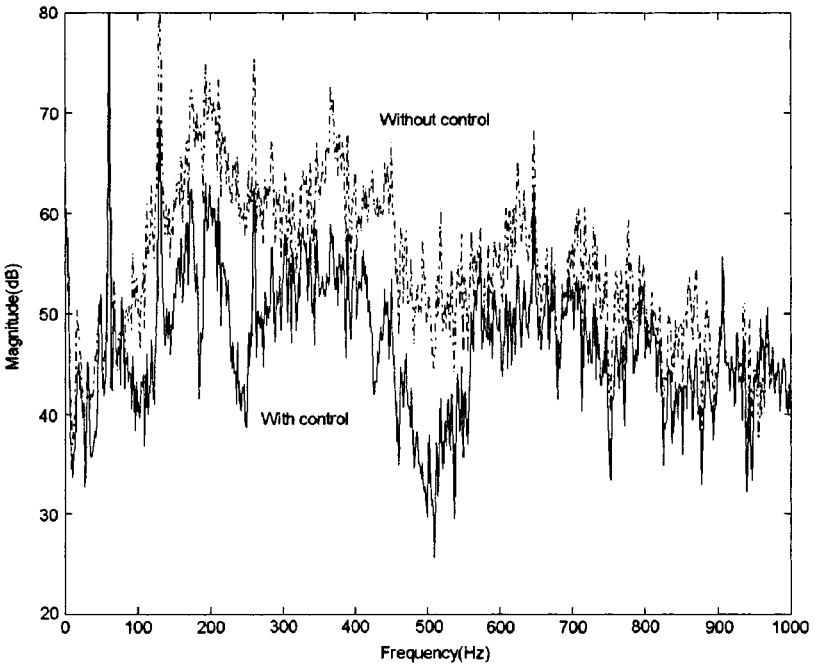

Fig. 17. Broad-band results of the feedforward active control in the duct (downstream boundary covered with bubble floss).

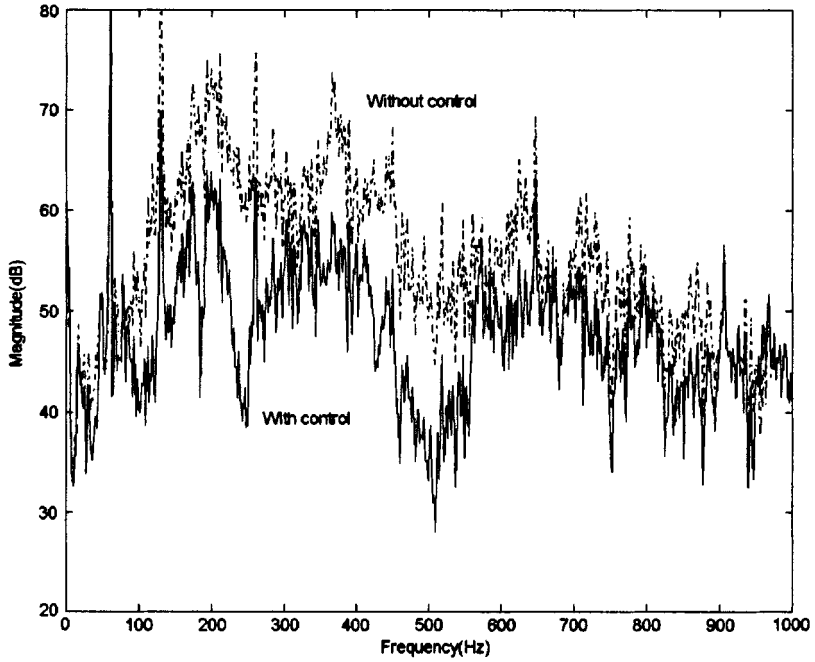

Fig. 18. Broad-band results of the feedforward active control in the duct (downstream boundary covered with a wind screen).

$$\times \frac{(1+5.8820z^{-1}+13.2152z^{-2})}{(1-1.7141z^{-1}+0.9659z^{-2})} \times \frac{(1-1.4598z^{-1}+0.9371z^{-2})}{(1-1.8546z^{-1}+0.9446z^{-2})} \times \frac{(1-1.1999z^{-1}+0.6563z^{-2})}{(1-0.6967z^{-1})} \times (1-1.7097z^{-1}+0.9596z^{-2}) \times (1-1.8777z^{-1}+0.9384z^{-2}) \times (1-1.8275z^{-1}+0.9325z^{-2}). \quad (5.7)$$

The optimal value of J in this case is 0.001 575 which is below the uncertainty bound given in (5.5). This value is then used as the estimated uncertainty bound, i.e., $\bar{\sigma} = 0.001\,575$ [see (4.21) and (4.22)].[1] Finally, the upper and lower bound of k ((5.4)) can be calculated from (4.22) as $\underline{k} = 0.023\,86$ and $\bar{k} = 0.146\,75$.

[1]In this experiment, we did not consider the model uncertainty induced from identification errors. There is a chance that (5.5) will be violated. In that case, one can redesign $\varepsilon(s)$ in (5.3) to give a more relaxed upper bound.

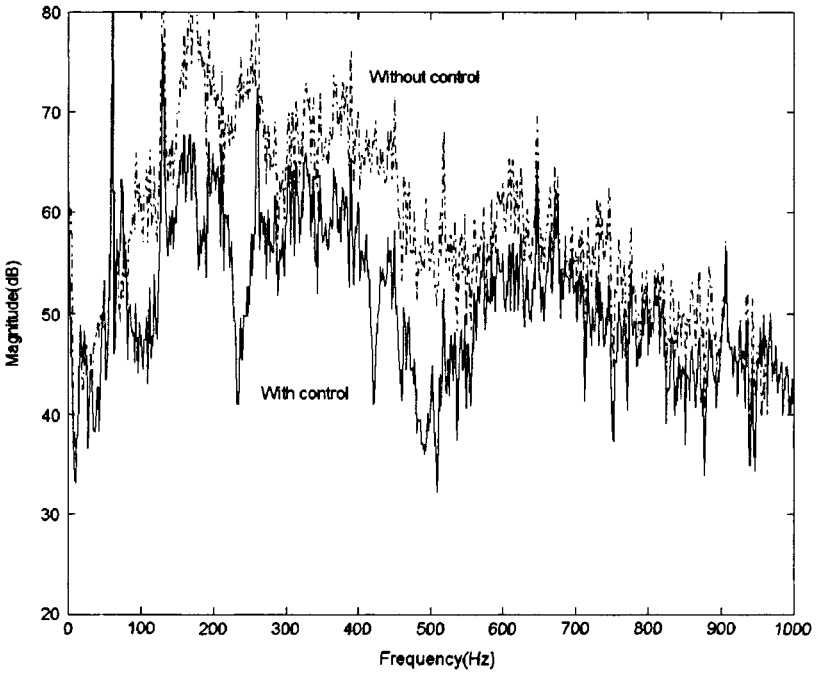

Fig. 19. Broad-band results of the feedforward active control in the duct (250 cm duct's length).

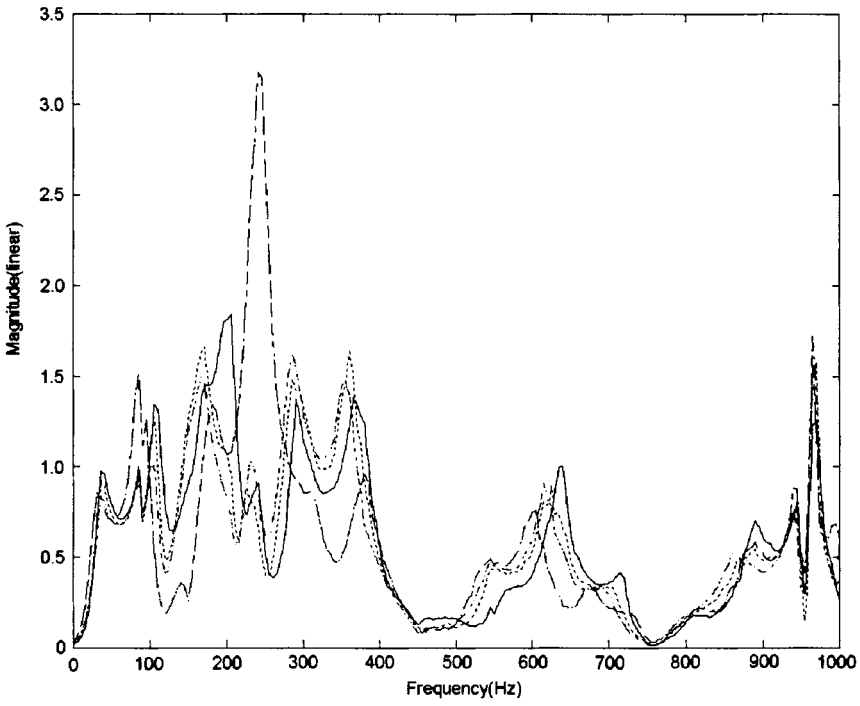

Fig. 20. Magnitude response from primary source to the upstream sensor with different boundary conditions, (solid line) boundary at $x = L$ is open, (dashed) the duct's length is changed, (dash dot) boundary at $x = L$ is filled with bubble floss, (dot) boundary at $x = L$ is filled with wind screen.

B. Experimental Results

Equation (5.4) was implemented on the duct Fig. 11 by setting $k = 0.0853$ (the mid-point between $\underline{k}$ and $\bar{k}$). A pseudo random noise was generated to test the effect of noise reduction. Fig. 16 shows the noise spectrum measured at a downstream location (see Fig. 11). The result indicates a significant broad-band reduction within the control bandwidth.

The robustness of the control law is dependent upon the phase of the transfer function $T(s)$ [(4.13)]. Further, as explained in Remark 4.1, the phase could possibly remain in the acceptable region when the downstream boundary changes. In other words, the controller designed in the experiment may still work for different boundaries at the duct's outlet. One can repeat the same procedure as described in Section IV for a precise check. In this

paper, we simply present the results directly, i.e., changing the boundary condition and duct's length as follows:

1) the boundary at $x = 200$ cm is covered with bubble floss;
2) the boundary at $x = 200$ cm is covered by a wind screen;
3) the duct's length is changed from 200 cm to 250 cm and the boundary at outlet is open.

Figs. 17–19 show the cancellation performance, all using the same controller. As a final note, the changes made in 1)–3) could drastically change the behavior of the dynamic if the measurement is taken at a single point. Fig. 20 shows the transfer functions between the control input and the microphone 1 (see Fig. 11) of the cases tested. The difference at certain frequency range could be quite large. Therefore, from the control system viewpoint, the two-sensor measurement has the effect of reducing the uncertainty. This advantage, however, does not appear in the design process if the wave propagation properties were not observed (e.g., using a lumped parameter model).

VI. Conclusion

A study of active noise cancellation in finite-length ducts using a feedforward structure is presented in this paper. The feedforward signal is the unidirectional wave obtained by a two-sensor measurement. Since the feedforward signal contains the influence from the actuator, the overall system can be cast as a feedback control problem from the time-domain perspective. It is shown that the ideal control law needs modification in the presence of measurement noise and model uncertainty. A frequency-domain based design procedure is proposed to calculate the modified control law. An experimental procedure is described to implement the proposed design and results are demonstrated. Further, experiments with different boundary conditions and duct lengths were conducted to verify the robustness of the control law.

References

[1] B. A. Francis, "On the Wiener-Hopf approach to optimal feedback design," *Syst. Contr. Lett.*, vol. 2, no. 4, pp. 197–201, Dec. 1982.

[2] K. Eghtesadi and H. G. Leventhall, "Active attenuation of noise—The monopole system," *J. Acoust. Soc. Amer.*, vol. 71, no. 3, pp. 608–611, 1982.

[3] L. J. Eriksson, M. C. Allie, and R. A. Greiner, "The selection and application of an IIR adaptive filter for use in active sound attenuation," *IEEE Trans. Acoust., Speech, Signal Processing*, vol. ASSP-35, pp. 433–437, Apr. 1987.

[4] R. F. La Fontaine and I. C. Shepherd, "An experimental study of a broadband active attenuator for cancellation of random noise in ducts," *J. Sound Vibration*, vol. 91, no. 3, pp. 351–362, 1983.

[5] C. R. Fuller, C. A. Rogers, and H. H. Robertshaw, "Control of sound radiation with active adaptive structures," *J. Sound Vibration*, vol. 157, pp. 19–39, 1992.

[6] M. E. Halpern, "Preview tracking for discrete-time SISO systems," *IEEE Trans. Automat. Contr.*, vol. 39, pp. 589–592, Mar. 1994.

[7] J. Hong, J. C. Akers, R. Venugopal, M. N. Lee, A. G. Sparks, P. D. Washabaugh, and D. S. Bernstein, "Modeling, identification, and feedback control of noise in an acoustic duct," *IEEE Trans. Contr. Syst. Technol.*, vol. 4, pp. 283–291, May 1996.

[8] J. Hu, "Active sound attenuation in finite-length ducts using close-form transfer function models," *ASME J. Dynamic Syst., Measurement Contr.*, vol. 117, no. 2, pp. 143–154, 1995.

[9] "Active noise cancellation in ducts using internal model-based control algorithms," *IEEE Trans. Contr. Syst. Technol.*, vol. 4, pp. 163–170, Mar. 1996a.

[10] "Feedforward and feedback control strategy for active noise cancellation in ducts," *ASME J. Dynamic Syst., Measurement, Contr.*, vol. 118, no. 2, pp. 372–378, 1996b.

[11] J. Hu, S. H. Yu, and C. S. Hsieh, "Application of model-matching techniques to feedforward active noise controller design," *IEEE Trans. Contr. Syst. Technol.*, vol. 6, pp. 33–42, Jan. 1998.

[12] A. J. Hull, C. J. Radcliffe, and S. C. Southward, "Global active noise control of a one-dimensional acoustic duct using a feedback controller," *ASME J. Dynamic Syst., Measurement Contr.*, vol. 115, pp. 488–494, 1993.

[13] M. J. M. Jessel and G. A. Mangiante, "Active sound absorbers in an air duct," *J. Sound Vibration*, vol. 23, no. 3, pp. 383–390, 1972.

[14] S. M. Kuo and D. R. Morgan, *Active Noise Control Systems—Algorithms and DSP Implementations*. New York: Wiley, 1996.

[15] P. Lueg, "Process of Silencing Sound Oscillations," U.S. Patent 2 043 416, 1936.

[16] P. A. Nelson and S. J. Elliott, *Active Control of Sound*. New York: Academic, 1992.

[17] A. D. Pierce, *Acoustics: An Introduction to Its Physical Principles and Applications*. New York: McGraw-Hill, 1981, pp. 107–113.

[18] R. Shoureshi, L. Brackney, N. Kubota, and G. Batta, "A modern control approach to active noise control," *ASME J. Dynamic Syst., Measurement, Contr.*, vol. 115, pp. 673–678, Dec. 1993.

[19] M. A. Swinbanks, "The active control of sound propagation in long ducts," *J. Sound Vibration*, vol. 27, no. 3, pp. 411–436, 1973.

[20] T. C. Tsao, "Optimal feedforward digital tracking controller design," *ASME J. Dynamic Syst., Measurement, Contr.*, vol. 116, pp. 583–592, Dec. 1994.

[21] G. E. Warnaka, L. A. Poole, and J. Tichy, "Active Acoustic Attenuator," U.S. Patent 4 473 906, Sept. 1984.

[22] B. Widrow and S. D. Stearns, *Adaptive Signal Processing*. Englewood Cliffs, NJ: Prentice-Hall, 1985.

Jwusheng Hu received the B.S. degree from the Department of Mechanical Engineering, National Taiwan University, Taiwan, in 1984, and the M.S. and Ph.D. degrees from the Department of Mechanical Engineering, University of California at Berkeley, in 1988 and 1990, respectively.

He is currently and Professor in the Department of Electrical and Control Engineering, National Chiao-Tung University, Taiwan. His current research interests include active noise control, software engineering for real-time control, and applications of digital signal processors.

Jyh-Feng Lin received the B.S. degree from the Department of Mechanical Engineering, National Taiwan University, Taiwan, in 1984, and the M.S. degree from the Institute of Aeronautics and Astronautics, National Cheng Kung University, Taiwan, in 1986. He is currently working toward the Ph.D. degree at the Department of Electrical and Control Engineering, National Chiao-Tung University, Taiwan.